Impacts of the Pacific Meridional Mode on June-August Precipitation in the Amazon River Basin

Wei Zhang[1*], Gabriele Villarini[1], and Gabriel A. Vecchi[2,3]

[1]IIHR-Hydroscience & Engineering, The University of Iowa, Iowa City, Iowa, USA

[2]Atmospheric and Oceanic Sciences Program, Princeton University, Princeton, NJ, USA

[3]National Oceanic and Atmospheric Administration/Geophysical Fluid Dynamics Laboratory, Princeton, NJ, USA

Revision submitted to Quarterly Journal of the Royal Meteorological Society

*Corresponding author:

Wei Zhang, Ph.D.

IIHR-Hydroscience & Engineering, The University of Iowa, Iowa City, Iowa, USA

Email: wei-zhang-3@uiowa.edu

This is the author manuscript accepted for publication and has undergone full peer review but has not been through the copyediting, typesetting, pagination and proofreading process, which may lead to differences between this version and the Version of Record. Please cite this article as doi: 10.1002/qj.3053

Abstract

This study examines the impacts of the Pacific Meridional Mode (PMM) on Amazon precipitation during the June-August months using observations and several experiments with the National Oceanic and Atmospheric Administration/Geophysical Fluid Dynamics Laboratory (NOAA/GFDL) Forecast-oriented Low Ocean Resolution Version of CM2.5 (FLOR). We find that the positive (negative) PMM can lead to precipitation surplus (deficit) using both observations and climate simulations with FLOR. The impacts of PMM on Amazon precipitation during June-August are induced by the forcing of sea surface temperature (SST) anomalies associated with PMM. Positive PMM can force the baroclinic Gill responses to the heat source in the Pacific with two low-level cyclones (anticyclones) located west (east) of the heating source. The anomalous low-level anticyclone and high-level cyclone located in the Amazon region are associated with low-level moisture moisture transport from the Atlantic. There is significant positive correlation between the PMM index and moisture flux convergence in most part of the Amazon basin, with negative correlation in its northwestern part. Such physical mechanisms underlying the linkage between PMM and the Amazon precipitation are supported by both the 500-year control experiment and a suite of perturbation experiments with FLOR.

1. **Introduction**

The Amazon River Basin accounts for ~20% of the fresh water on the earth while the Amazon rainforest produces approximately 10% of land productivity and biomass (Joetzjer et al. 2013). Overall, the Amazon Basin plays an important role in the global climate, regulating global water and carbon cycles (Foley et al. 2002). The severe Amazon drought events in 2005 and 2010 have attracted large attention due to the extensive damage to the rainforest and people (e.g., Zeng et al. 2008; Yoon and Zeng 2010; Lewis et al. 2011; Marengo et al. 2011; Marengo and Espinoza 2016). Because of the regional and global effects that drought in this area has, it is therefore critical to better understand the physical mechanisms underlying Amazon precipitation variability which is closely associated with droughts.

The rainfall in the Amazon basin is characterized by a marked seasonal cycle tied with seasonal change of low-level jets (LLJ) and sea surface temperature (e.g., Figueroa and Nobre, 1990; Zeng 1999; Li et al. 2006; Espinoza et al. 2009). In addition, the Amazon precipitation is strongly tied to the seasonal migration of the inter-tropical convergence zone (ITCZ) (e.g., Foley et al. 2002; Cook and Vizy 2008) with remarkable seasonal precipitation changes, with summers that are characterized by large amounts of precipitation over this area, while the precipitation in winter is more localized in the northern and western parts (Ronchail et al. 2002).

Previous studies have found that different climate modes can modulate Amazon precipitation, with particular emphasis on the El Niño–Southern Oscillation (ENSO) (e.g., Foley et al. 2002; Grimm 2003; Li et al. 2011a; Marengo 1992; Richey et al. 1989; Tedeschi and

Collins 2016). The tropical Atlantic sea surface temperature (SST) patterns (e.g., warming, cooling and SST gradient) can also strongly modulate Amazon precipitation (e.g., Cox et al. 2008; Enfield 1996; Good et al. 2008; Lewis et al. 2011; Marengo et al. 2011; Nobre and Shukla 1996; Yoon and Zeng 2010; Zeng et al. 2008) because the changes in the meridional gradient of SST in the tropical Atlantic may influence the pattern of moisture convergence, vertical motion, and ITCZ (Aceituno 1988; Good et al. 2008; Kousky et al. 1984; Marengo et al. 2011). In particular, the tropical North Atlantic warming was found to trigger and develop the 2010 Amazon drought event (Lewis et al. 2011; Marengo et al. 2011). In addition, the southern tropical Atlantic has also been highlighted as a potential source of inter-annual precipitation variability (Yoon and Zeng 2010; Satyamurty et al 2013a).

The influences of SST anomalies in both the Pacific and Atlantic Oceans on the Amazon precipitation also depend on seasonality and regions. The rainfall in the Amazon basin is characterized by a strong spatial contrast, particularly in the western part of the basin (Poveda et al., 2014; Espinoza et al, 2015). The extreme floods in the southwestern Amazon basin have been related to SST anomalies in the Indo-Pacific ocean and in the sub-tropical south Atlantic ocean (Ronchail et al., 2005; Espinoza et al., 2014; Cavalcanti et al., 2016). There are particular influences of SST anomalies in the central Pacific and north tropical Atlantic on rainfall in the Andean/Amazon region (e.g. Espinoza et al., 2011; 2013; Lavado-Casimiro et al 2013). The northeastern Amazon precipitation is largely modulated by ENSO while the southwestern part by the Atlantic SST (Aceituno 1988; Tedeschi et al. 2013; Satyamurty et al 2013a; Zou et al. 2016).

However, the correlation between precipitation in the equatorial western Amazon and the Pacific and Atlantic SST is relatively weak (Enfield 1996). Moreover, the seasonality of SSTs in the tropical Pacific and Atlantic Oceans has a profound influence on precipitation in the eastern Amazon during the equinox seasons (i.e., March and September) via the influence of ITCZ (Andreoli et al. 2016; Fu et al. 2001; Grimm 2003; Tedeschi and Collins 2016) and on precipitation in the western Amazon by modulating the Walker Circulation and Handley cell (Espinoza et al. 2016).

Several studies have identified ENSO as a major driver of precipitation over the Amazon Basin. A climate mode that is strongly tied to ENSO but that has not received much attention in relation to precipitation over this region is the Pacific Meridional Mode (PMM). PMM is the first Singular Value Decomposition (SVD) of SST and the zonal and meridional components of the 10m wind fields (Chiang and Vimont 2004). PMM is strongly tied with the development of ENSO and the changes in large-scale circulation (Chang et al. 2007; Larson and Kirtman 2013, 2014; Yu et al. 2014; Zhang et al. 2009). Moreover, PMM strongly modulates the occurrence of tropical cyclones in the western North Pacific and eastern Pacific (Collins et al. 2016; Murakami et al. 2016; Zhang et al. 2016; 2017) and the precipitation changes in East Asia by exciting teleconnections (Li et al. 2011b). PMM, as a typical climate mode in the subtropical and tropical eastern Pacific affecting large-scale circulation, may therefore influence precipitation variability in the Amazon region. This study aims to assess whether, the extent to which and why PMM

modulates precipitation in Amazon and can advance our understanding of precipitation variability and droughts in the Amazon Basin.

This paper is organized as follows. Section 2 presents the data and methodology, while Section 3 discusses the results based on observations and simulations. Section 4 includes the discussion and summarizes the main conclusions.

2. Data and Methodology

2.1 Data

As reference dataset we use the global gridded terrestrial precipitation data from the Multi-Source Weighted-Ensemble Precipitation (MSWEP) project (Beck et al. 2017). This product is obtained by merging rain gauge, satellite, and reanalysis data from seven datasets: two gauge observations [Climate Prediction Center (CPC) Unified and Global Precipitation Climatology Centre (GPCC)], three satellite data products [CPC MORPHing technique (CMORPH), Global Satellite Mapping of Precipitation (GSMaP-MVK), and Tropical Precipitation Measuring Mission (TRMM) Multi-satellite Precipitation Analysis (TMPA) 3B42RT], and two atmospheric model reanalysis data (the European Center for Medium range Weather Forecasting (ECMWF) ReAnalysis (ERA)-Interim and the Japanese 55-year Reanalysis (JRA-55)). This dataset covers the period 1979–2014 with a 3-hourly temporal and 0.25° spatial resolution. The long-term climatology of MSWEP is based on the Climate Hazards Group's Precipitation Climatology version but adjusted with more accurate regional datasets if available. Gauge under-catch and orographic effects have been globally corrected by inferring catchment-

average precipitation from streamflow observations at 13762 stations. The SST data are downloaded from the Met Office Hadley Center (HadISST, version 1.1; Rayner et al. 2003). The surface wind data are obtained from the NCEP/National Center for Atmospheric Research (NCAR) reanalysis project (NCEP-NCAR; Kalnay et al. 1996).

2.2 Methods: PMM and Partial Correlation

The PMM index is processed following Chiang and Vimont (2004). The PMM index is calculated by applying maximum covariance analysis (MCA)/singular value decomposition (SVD) to monthly SST and surface wind in the region [32ºN–21ºS and 175ºE–95ºW] as follows. The seasonal cycle and the linear fit to the cold tongue index (Deser and Wallace 1987) is removed from the SST and surface wind data, followed by applying a three-month running average. Specifically, we subtract the linear least squares fit to a commonly-used ENSO index (e.g., cold tongue index) which is defined as the SST anomalies averaged over [6ºS–6ºN and 180º – 90ºW] from all the fields which are used to calculate the PMM index. By doing this, we remove the linear impacts of ENSO on PMM. We then apply MCA/SVD to the cross-covariance matrix between SST and both components of 10-m winds to extract the leading mode of coupled variability. The PMM index is the monthly expansion coefficient of the leading mode (SST/wind). The spatial pattern of PMM is obtained by regressing the SST and wind fields onto the normalized SST expansion coefficients in the region [32ºN–21ºS and 175ºE–95ºW].

To further control the impacts of ENSO on the linear relation between PMM and precipitation, we calculate the partial correlation between PMM and precipitation by controlling for ENSO. The equation for partial correlation is:

$$\rho_{xy\cdot z} = \frac{\rho_{xy-}\,\rho_{xz\cdot}\rho_{yz\cdot}}{\sqrt{1-\rho_{xz}^2}\sqrt{1-\rho_{yz}^2}}$$

where x, y, z represent precipitation, PMM and the ENSO index respectively; ρ_{xy} represents the correlation between PMM and precipitation at each grid, ρ_{xz} represents the correlation between ENSO and precipitation at each grid, ρ_{yz} represents the correlation between PMM and ENSO while $\rho_{xy\cdot z}$ represents the correlation between PMM and precipitation by controlling ENSO.

2.3 Methods: Climate Model and Experiments

We use the NOAA/Geophysical Fluid Dynamics Laboratory (NOAA/GFDL) Forecast-oriented Low Ocean Resolution Version of CM2.5 (FLOR) (Vecchi et al. 2014) to perform control and perturbation experiments. The ocean component of FLOR has a spatial resolution of 1º× 1º while the atmospheric and land components have a 0.5º × 0.5º spatial resolution (Vecchi et al. 2014).

We analyze the association between Amazon precipitation and PMM in the present-day control run by prescribing radiative forcing and land-use representative of 1990 using FLOR with flux adjustments (FLOR-FA 1990). This is a fully-coupled free run with FLOR-FA in which no SST is prescribed.

We also perform two experiments to examine the net impacts of PMM on forcing the precipitation changes in the Amazon River Basin. In the control experiment (CTRL), SST is restored to a repeating annual cycle of the SST climatology of the FLOR 1860 control run with a ten-day restoring timescale (*tau*). The perturbation experiment is performed by prescribing the sum of the annual cycle of SST climatology of the FLOR 1860 control run and the temporally constant SST anomalies associated with the positive PMM patterns (denoted as PPMM) at the same time scale. The SST-restoring experiments are defined as follows. The restoring of SST in the model to the observed estimates is represented by:

$$\frac{dT}{dt} = \xi + \frac{T(obs) - T(model)}{tau} \quad (1)$$

where ξ is the SST tendency in the coupled model, tau is the constant restoring time scale (e.g., 5-day or 10-day), dT represents the change of SST and dt change of time; T(obs) represents a space- and time-dependent array of the observed estimates of SST whereas T(model) is the SST simulated by the model. The larger the tau, the more relaxed the coupling and the weaker the nudging/restoring of SST. A fully-coupled free run has a tau of infinity while an Atmospheric Model Intercomparison Project (AMIP) run has a tau of zero. The restoring time scale is set as ten-day because this partially allows the changes of simulated SST, which is different from AMIP runs in which SST is considered as boundary forcing and cannot be changed.

After an initial 100-year spinup, both experiments (CTRL and PPMM) are integrated for 60 years. The subtraction of the CTRL experiment from the perturbation experiment represents the responses of the climate system to PPMM.

2.4 Methods: Dynamic linkage between PMM and precipitation

We use the changes of moisture flux and relevant derived variables to diagnose the precipitation variability in the Amazon Basin (Marengo 2005; Zeng 1999). We start with the atmospheric moisture budget equation:

$$\frac{dW}{dt} = -P + E + C \quad (2)$$

where W is the precipitable water in the atmospheric column, t is time, P is precipitation, E is evaporation and C is the convergence of vertically integrated moisture which can be written as:

$$\mathrm{C} = -\nabla \cdot \mathrm{Q} \quad (3)$$

where Q is the vertically integrated water-vapor (moisture) flux and ∇ is the horizontal gradient operator. Moisture flux (Q) is represented by:

$$\mathrm{Q} = \frac{1}{g}\int_{Pu}^{Ps} qV\, dp \quad (4)$$

where q is the specific humidity (kg/kg), V denotes wind vector, g is the gravitational constant, and P_u and P_s denote the 300 and 1000 hPa pressure levels, respectively.

At the seasonal scale, the term $\frac{dW}{dt}$ denotes the precipitable water change and is basically negligible (zero) for monthly or seasonal averages because changes in $\frac{dW}{dt}$ are small at these scales and longer (Costa and Foley 1999; Marengo 2005; Zeng 1999). Therefore, the moisture budget equation can be simplified as:

$$P - E\,HC = -\nabla \cdot Q \quad (5)$$

which suggests that precipitation (out of) is nearly equal to the sum of the moisture converged into the atmospheric column (into) and the water vapor evaporated into it (inside of the atmospheric column) (Marengo 2005; Werth and Avissar, 2004; Zeng 1999; Juárez et al. 2007; Trenberth et al. 2011). This suggests that the moisture flux convergence/divergence anomalies can be used to diagnose the precipitation surplus/deficit in the Amazon region (Satyamurty et al. 2013b).

Following Helmholtz theorem, the vertically integrated water vapor flux is decomposed into the non-divergent (rotational) component and the divergent (irrotational) component, which can be derived from the moisture flux streamfunction (ψ_Q) and the moisture flux potential ($\mathcal{X}_Q$) (Chen 1985; Rosen et al. 1979):

$$Q = Q_\psi + Q_\mathcal{X} = \vec{k} \cdot \nabla\psi_Q + \nabla\mathcal{X}_Q \quad (6)$$

where Q_ψ and $Q_\mathcal{X}$ represent the divergent and rotational component of water vapor flux (Q) respectively, and $\vec{k}$ is the unit vector in the direction of the z-axis.

The quantities ψ_Q and χ_Q have been widely used to diagnose the relationship between the atmospheric circulation and moisture convergence/transport (Chen 1985; Rosen et al. 1979; Wang et al. 2010, 2011; Wang and Clark 2010):

$$\psi_Q = \nabla^{-2}\left(\overrightarrow{k} \cdot \nabla \times Q\right) \quad (7)$$

$$\chi_Q = \nabla^{-2}(\nabla \cdot Q) \quad (8)$$

where ψ_Q represents the moisture flux streamfunction; $\overrightarrow{k}$ is the unit vector in the direction of the z-axis; χ_Q denotes the moisture flux potential which is related to the source and sink of water vapor through the water vapor balance equation; ∇^{-2} denotes the Laplace inverse transform operator. The term ψ_Q has been widely used to illustrate large-scale transport of water vapor (Chen 1985), and it therefore supports the analysis of moisture flux transport associated with precipitation change in the Amazon basin. This study will use moisture flux streamfunction (ψ_Q) and potential χ_Q to diagnose precipitation change in the Amazon basin.

2.5 Methods: Seasonal Change of Amazon Precipitation

The climatology of precipitation in South America is shown in Figure 1. The Amazon region receives the most precipitation in December-February (DJF), followed by March-May (MAM). The months from June to August (JJA) represent the driest season over the basin, though the northern edge (close to the equator) receives large amounts of precipitation during JJA. Overall, the precipitation in the Amazon River Basin during September-November (SON) is more than that in JJA (Figure 1). In general, the period from June to November is considered as

the dry season for this region in terms of the proportion of precipitation and total precipitation (Figure 1). A strong precipitation deficit in the dry season indicates a high risk of drought over this area. For example, the severe 2010 drought began with a strong El Niño event in DJF and was intensified by the tropical North Atlantic warming in the following months (Marengo et al. 2011).

3. Results

PMM is characterized by a meridional pattern of SST and coupled 10-m surface wind fields (Figure 2). The observed typical PMM pattern is featured by warming (cooling) in the northern (southeastern) part of the PMM region [32ºN–21ºS and 175ºE–95ºW] (Figure 1a). The simulated PMM pattern (Figure 2b) with FLOR-FA 1990 control run (500 years) captures the fundamental structure present in the observations, though the SST cooling part is weaker. Moreover, the surface wind coupled with the SST cooling of the PMM pattern in FLOR-FA 1990 control run is also slightly weaker than in the observations. This is consistent with the simulated PMM pattern in the FLOR-FA 1860 control experiment (Zhang et al. 2016; 2017).

The correlation between the PMM index and JJA precipitation over South America in observations is shown in Figure 3. The Amazon precipitation has a significant positive correlation with the PMM index during JJA (Figure 3a), suggesting that there is anomalous precipitation surplus (deficit) during positive (negative) PMM phases in this region. Meanwhile, significant positive correlation is also observed in the eastern part of South America (Figure 3a).

The PMM pattern is partially collocated with ENSO in the tropical Pacific. Previous studies have argued that the PMM is largely followed by ENSO in the tropical Pacific (Chang et al. 2007; Larson and Kirtman 2013, 2014; Yu et al. 2014; Zhang et al. 2009). It is therefore reasonable to examine whether the association between Amazon precipitation and PMM is influenced by ENSO. Although the linear impacts of ENSO has been removed when calculating the PMM index, we analyze the partial correlation by controlling for two ENSO indices (Niño3.4 and Niño4) to further isolate the impacts of ENSO. The partial correlation between PMM and precipitation by controlling Niño3.4 and Niño4 indices (Figure 3, panels b and c) remains largely unaltered when compared with what obtained by regressing precipitation on PMM (Figure 3a), suggesting that the association between PMM and Amazon precipitation in JJA is robust and is weakly influenced by ENSO. The values of PMM averaged over JJA for the drought events in 1997/1998, 2005, and 2010 were all negative, consistent with the results in Figure 3. The time series of the PMM index and average precipitation over the Amazon basin during June-August is shown in Figure 4. The correlation between the two time series is 0.52, significant at 0.01 level, supporting the significant positive spatial correlation in Figure 3.

3.1 Physical Mechanisms

PMM is a coupled mode of SST and surface winds, which can drive changes in large-scale circulation by teleconnections (e.g., Collins et al. 2016; Li et al. 2011b; Murakami et al. 2016; Zhang et al. 2016). Moisture flux convergence/divergence is a good indicator to diagnose precipitation. In addition, moisture flux streamfunction (ψ_Q)/potential (χ_Q) and its non-

divergent/divergent components are also used to diagnose precipitation changes. In addition, the moisture source for the Amazon basin is mainly from the North Atlantic in both wet and dry seasons (Satyamurty et al, 2013a,b; Drumond et al. 2014). The moisture transport from the North Atlantic is also used to diagnose precipitation change in this study.

Figure 5 shows the correlation map between the PMM index and moisture flux convergence in the Amazon basin. There is positive correlation between PMM and moisture flux convergence in most part of the Amazon basin, suggesting that the positive PMM phase is tied with positive moisture flux convergence anomalies, which tend to cause more precipitation based on water vapor budget (see equation (5) and Figure 5). However, there is negative correlation between the PMM index and moisture flux convergence in the northwestern part of the Amazon basin (Figure 5) where the correlation between the PMM index and precipitation (Figure 3) is mostly positive. This discrepancy needs further investigation.

Figure 6a illustrates the regression of moisture flux convergence onto the PMM index during JJA. Strong moisture convergence anomalies represented by positive moisture potential are located in the tropical central Pacific where the warming part of the positive PMM pattern is collocated and over the Amazon region (Figure 6a). An anomalous moisture convergence over this area during JJA suggests precipitation surplus. In addition, the moisture flux convergence/divergence is mainly caused by low-level flow convergence/divergence (e.g., 850 hPa). Figure 6b shows the 850-hPa velocity potential and divergent wind, which strongly resemble those of moisture flux (Figure 6a), supporting the key role of low-level

convergence/divergence in causing the moisture flux convergence/divergence. Therefore, the positive (negative) PMM phase is associated with anomalous moisture convergence (divergence) over the Amazon region, which is related to anomalous precipitation surplus (deficit). To further diagnose the physical mechanisms, we analyze the moisture streamfunction and low- and high-level of streamfunction and rotational wind related to PMM. Figure 7a shows the regression of moisture streamfunction and rotational component onto the PMM index during JJA. Moisture streamfunction has a remarkable spatial pattern with negative/positive streamfunction anomalies over South America/North Atlantic, respectively. Accompanying the streamfunction anomalies, there is strong moisture transport (non-divergent component of the moisture flux) from the Equatorial Atlantic into the Amazon basin (Figure 7a). Previous studies have found that the moisture source for the Amazon basin is mainly from the North Atlantic in both wet and dry seasons (Satyamurty et al, 2013a,b; Drumond et al. 2014).

There are two nearly symmetric anticyclonic patterns of moisture flux straddling over the equator. In the Pacific Ocean, there is also a symmetric flow pattern characterized by two cyclones located west of the date line (Figure 7b). The two symmetric cyclonic (anticyclonic) moisture flux centers west (east) of the PMM-related forcing are quite similar to the classic baroclinic Gill responses of low-level large-scale circulation to the heat source in the tropics (Gill 1980; Lee et al. 2009). The regression of low-level 850-hPa streamfunction and rotational wind onto PMM is almost the same as that of moisture flux (Figure 7b). Moreover, the regression of upper level (200-hPa) streamfunction and rotational wind onto PMM is the

opposite of that for lower level (850-hPa), suggesting a marked baroclinic structure that supports the classic baroclinic Gill responses to the heat source associated with PMM (Figure 7c). Therefore, the positive (negative) PMM may force the baroclinic Gill responses of the large-scale circulation to the east and west sides. We hypothesize that this 'Gill response' may contribute to anomalous moisture convergence (divergence) over the Amazon region which is related to anomalous precipitation surplus (deficit) there during the positive (negative) PMM phase. However we have not investigated the possible interaction between rotational and divergent moisture transport nor the dependence of any such interaction on the PMM.

3.2 Results based on GFDL FLOR

Up to this point, we have focused on diagnosing the physical mechanisms underlying the PMM-Amazon precipitation association during JJA using observations. Here we further support these insights using the results based on GFDL FLOR experiments.

The observed association between Amazon precipitation and the JJA PMM index is supported by the 500-year FLOR-FA 1990 control experiment which is a fully-coupled free run (Figure 8a). The precipitation over this basin has a significant positive correlation with the PMM index in the long FLOR-FA 1990 experiment, consistent with what found in the observations (Figure 3). This indicates that the observed association between Amazon precipitation and JJA PMM index also holds in a long fully-coupled climate simulation.

Further, we perform a pair of experiments to test the net influence of the positive PMM phase: the control experiment (CTRL; refer to Section 2 for more details about the experiments) and the perturbation experiment which prescribes the SST anomalies in the positive PMM phase (PPMM). The PPMM experiment produces a positive precipitation anomaly over the Amazon Basin, further corroborating the impacts of PMM on Amazon precipitation during JJA (Figure 8b).

The physical mechanisms underlying the linkage between PMM and Amazon precipitation during JJA in the observations are also supported by the long control experiment with FLOR (Figure 9). The regression of moisture flux streamfunction and rotational components onto PMM in FLOR-FA 1990 control experiment bears strong resemblance to that in the observations (Figure 9a). There are two symmetric cyclones (anticyclones) west (east) of the PMM region (Figure 9a), supporting the classic Gill responses to the heat source in the observations (Figure 9). There is strong easterly component along the eastern part of the Amazon basin associated with the two symmetric anticyclones. Such easterly component of moisture flux plays a crucial role in transporting moisture from the Atlantic to the Amazon basin, similar to those in observations (Figure 7a). We hypothesize that such rotational easterly moisture transport related to positive PMM may be associated with the precipitation change in the Amazon basin, but we have not investigated this point in detail. The regression of moisture flux potential and divergent components onto PMM with FLOR-FA 1990 control experiment are also similar to the observations (Figure 9b) in which there is moisture flux convergence in the Pacific and the

Amazon region. This suggests that the Amazon precipitation-PMM association and the underlying physical mechanisms in the observations are supported by the long FLOR-FA control experiments.

To further assess the causal relationship between PMM and Amazon precipitation, we analyze the differences in dynamical variables between PPMM and CTRL experiments. The subtraction of the CTRL experiment from the PPMM experiment represents the responses to the forcing of PPMM. The responses of moisture flux streamfunction and rotational components to positive PMM (PPMM minus CTRL) is almost the same as those in the FLOR-FA control experiment (Figures 9a and 10a), suggesting that the heat source associated with PPMM forces the Gill responses on its east and west sides. The responses of moisture flux potential and divergent components to PPMM bear strong similarity to those in the FLOR-FA 1990 control experiment with positive moisture flux convergence in the Amazon region characterized by positive moisture flux potential (Figure 10b). Therefore, the physical mechanisms underlying the observed association between PMM and JJA precipitation in the Amazon region are supported by the 500-year long control experiments and a pair of sensitivity experiments with GFDL FLOR climate model.

4. Discussion and Conclusion

The Amazon precipitation can be modulated by ENSO and Atlantic SST anomalies. The droughts events in 1997-1998, 2005, 2010 and 2015 have been attributed to SST warming in the

North Atlantic or strong El Niño events (Jiménez-Muñoz et al. 2016; Marengo and Espinoza 2016; Marengo et al. 2011). ENSO modulates the Amazon precipitation by altering the Walker circulation while the Atlantic SST anomalies influence Amazon precipitation by changing s the north-south divergent circulation and shifting the ITCZ and Hadley cell (Yoon and Zeng, 2010; Espinoza et al., 2016). The modulation of Amazon precipitation by the SST variability has dramatically advanced our understanding of the historical droughts/floods events.

We have examined the impacts of PMM on Amazon precipitation during June-August because the positive correlation between PMM and the Amazon precipitation is much weaker during other seasons; we have found that the positive (negative) PMM can lead to precipitation surplus (deficit) based on both observations and climate model simulations. There is significant positive correlation between the PMM index and moisture flux convergence in most of the Amazon basin, with negative correlation in the northwestern part of the Amazon basin. The impacts of PMM on the Amazon precipitation during June-August are induced by the forcing of SST anomalies associated with PMM. Positive PMM can force the baroclinic Gill responses to the heat source in the Pacific with two low-level cyclones (anticyclones) west (east) of the heat source. The anomalous low-level anticyclone and high-level cyclone located in the Amazon region are associated with moisture flux transport and convergence which leads to changes in precipitation over this basin. Such mechanisms are supported by both the long FLOR-FA 1990 control experiment and a pair of perturbation experiments (PPMM and CTRL).

The impacts of PMM on JJA Amazon precipitation identified in this study suggest that negative PMM can contribute to drought conditions in Amazon. However, the relative contributions by ENSO, Atlantic SST anomalies and PMM in the Amazon precipitation and droughts/floods are yet to be identified, and should be the subject of future studies.

This study has focused on the association between PMM and the Amazon precipitation during JJA because the positive correlation between PMM and the Amazon precipitation is much weaker during other seasons. Further investigation is required to assess why the association between PMM and the Amazon precipitation in JJA is stronger than those in other seasons. The impacts of PMM on the Amazon precipitation are different from those induced by El Niño and Atlantic SST anomalies in terms of region and physical mechanisms. The impacts of PMM on the Amazon rainfall is strong only during June-August while the impacts of ENSO are strong in all seasons with peaks in December to February (DJF, mature phase). The effects of ENSO on Amazon precipitation are more confined to the northeastern and western part of the Amazon (Ronchail et al., 2005; Aceituno 1988; Tedeschi et al. 2013; Espinoza et al., 2011; 2013, 2016; Zou et al. 2016) while those of Atlantic SST anomalies or SST gradient are located in the southwestern or northwestern part of the Amazon (Marengo and Espinoza 2016; Marengo et al. 2011). However, PMM exerts impacts on Amazon precipitation over the basin-wide Amazon region while the association between PMM and moisture flux convergence has negative correlation in the northwestern part of the Amazon basin (Figure 3a). PMM may be an important factor to consider in analyzing the variability of precipitation over the Amazon Basin, especially

during the JJA. Furthermore, a better understanding of precipitation variability over this area under the current climate can give more confidence to the projection of Amazon precipitation under climate change.

Acknowledgements:

The authors are grateful to the associate editor and two anonymous reviewers for insightful comments. This study was partly supported by Award NA14OAR4830101 from the National Oceanic and Atmospheric Administration, U.S. Department of Commerce.

References

Aceituno, P., 1988: On the functioning of the Southern Oscillation in the South American sector. Part I: Surface climate. Monthly Weather Review, 116, 505-524.

Andreoli, R. V., S. S. de Oliveira, M. T. Kayano, J. Viegas, R. A. F. de Souza, and L. A. Candido, 2016: The influence of different El Niño types on the South American rainfall. International Journal of Climatology, DOI: 10.1002/joc.4783.

Beck, H. E., A. I. J. M. van Dijk, V. Levizzani, J. Schellekens, D. G. Miralles, B. Martens, and A. de Roo, 2017: MSWEP: 3-hourly 0.25æglobal gridded precipitation (1979–2015) by merging gauge, satellite, and reanalysis data. Hydrol. Earth Syst. Sci. Discuss., 21, 589-615.

Cavalcanti, I. F. d. A., Marengo, J. A., Alves, L. M. and Costa, D. F. (2016), On the opposite relation between extreme precipitation over west Amazon and southeastern Brazil: observations and model simulations. Int. J. Climatol. doi:10.1002/joc.4942.

Chang, P., and Coauthors, 2007: Pacific meridional mode and El Niño—Southern Oscillation. Geophysical Research Letters, 34, L16608.

Chen, T.-C., 1985: Global water vapor flux and maintenance during FGGE. Monthly Weather Review, 113, 1801-1819.

Chiang, J. C. H., and D. J. Vimont, 2004: Analogous Pacific and Atlantic Meridional Modes of Tropical Atmosphere–Ocean Variability. Journal of Climate, 17, 4143-4158.

Collins, J. M., P. J. Klotzbach, R. N. Maue, D. R. Roache, E. S. Blake, C. H. Paxton, and C. A. Mehta, 2016: The record-breaking 2015 hurricane season in the eastern North Pacific: An analysis of environmental conditions. Geophysical Research Letters, 43, 9217-9224.

Cook, K. H., and E. K. Vizy, 2008: Effects of Twenty-First-Century Climate Change on the Amazon Rain Forest. Journal of Climate, 21, 542-560.

Costa, M. H., and J. A. Foley, 1999: Trends in the hydrologic cycle of the Amazon basin. Journal of Geophysical Research: Atmospheres, 104, 14189-14198.

Cox, P. M., and Coauthors, 2008: Increasing risk of Amazonian drought due to decreasing aerosol pollution. Nature, 453, 212-215.

Deser, C., and J. M. Wallace, 1987: El Niño events and their relation to the Southern Oscillation: 1925–1986. Journal of Geophysical Research: Oceans, 92, 14189-14196.

Drumond, A., J. Marengo, T. Ambrizzi, R. Nieto, L. Moreira, and L. Gimeno, 2014: The role of the Amazon Basin moisture in the atmospheric branch of the hydrological cycle: a Lagrangian analysis. Hydrology and Earth System Sciences, 18, 2577-2598.

Enfield, D. B., 1996: Relationships of inter‐American precipitation to tropical Atlantic and Pacific SST variability. Geophysical Research Letters, 23, 3305-3308.

Espinoza JC., J. Ronchail, J.L. Guyot, Cocheneau G., N Filizola, W. Lavado, E. deOliveira, R. Pombosa and P. Vauchel. 2009. Spatio – Temporal rainfall variability in the Amazon Basin Countries (Brazil, Peru, Bolivia, Colombia and Ecuador). International Journal of Climatology, 29, 1574-1594.

Espinoza, J. C., S. Chavez, J. Ronchail, C. Junquas, K. Takahashi, and W. Lavado, 2015: Rainfall hotspots over the southern tropical Andes: Spatial distribution, rainfall intensity, and relations with large-scale atmospheric circulation. Water Resources Research, 51, 3459-3475.

Espinoza JC., Ronchail J., Guyot J.L., Junquas C., Vauchel P., Lavado W.S., Drapeau G., Pombosa R. 2011: Climate variability and extremes drought in the upper Solimões River (Western Amazon Basin): Understanding the exceptional 2010 drought. Geophys. Res. Lett., 38, L13406, doi:10.1029/2011GL047862

Espinoza JC., Ronchail J., Frappart F., Lavado W., Santini W., Guyot JL. 2013: The major floods in the Amazonas River and tributaries (Western Amazon basin) during the 1970 – 2012 period: A focus on the 2012 flood. Journal of Hydrometeorology, 14, 1000-1008. doi: 10.1175/JHM-D-12-0100.1.

Espinoza JC. Marengo JA. Ronchail J. Molina J., Noriega L., Guyot JL. 2014: The extreme 2014 flood in south-western Amazon basin: The role of tropical subtropical south Atlantic SST gradient. Environm. Res. Lett. 9 124007 doi:10.1088/1748-9326/9/12/124007.

Espinoza, J. C., H. Segura, J. Ronchail, G. Drapeau, and O. Gutierrez-Cori, 2016: Evolution of wet-day and dry-day frequency in the western Amazon basin: Relationship with atmospheric circulation and impacts on vegetation. Water Resources Research, 52, 8546-8560.

Figueroa, S. N., and C. A. Nobre, 1990: Precipitation distribution over central and western tropical South America. Climanalise, 5, 36-45.

Foley, J. A., A. Botta, M. T. Coe, and M. H. Costa, 2002: El Nino–Southern oscillation and the climate, ecosystems and rivers of Amazonia. Global Biogeochemical Cycles, 16.

Fu, R., R. E. Dickinson, M. Chen, and H. Wang, 2001: How Do Tropical Sea Surface Temperatures Influence the Seasonal Distribution of Precipitation in the Equatorial Amazon? Journal of Climate, 14, 4003-4026.

Gill, A. E., 1980: Some simple solutions for heat-induced tropical circulation. Quarterly Journal of the Royal Meteorological Society, 106, 447-462.

Good, P., J. A. Lowe, M. Collins, and W. Moufouma-Okia, 2008: An objective tropical Atlantic sea surface temperature gradient index for studies of south Amazon dry-season climate variability and change. Philosophical Transactions of the Royal Society of London B: Biological Sciences, 363, 1761-1766.

Grimm, A. M., 2003: The El Niño impact on the summer monsoon in Brazil: regional processes versus remote influences. Journal of Climate, 16, 263-280.

Guttman, N. B., 1999: Accepting the standardized precipitation index: A calculation algorithm1. Wiley Online Library.

Jiménez-Muñoz, J. C., and Coauthors, 2016: Record-breaking warming and extreme drought in the Amazon rainforest during the course of El Niño 2015–2016. Scientific Reports, 6.

Joetzjer, E., H. Douville, C. Delire, and P. Ciais, 2013: Present-day and future Amazonian precipitation in global climate models: CMIP5 versus CMIP3. Climate Dynamics, 41, 2921-2936.

Juárez, R. I. N., M. G. Hodnett, R. Fu, M. L. Goulden, and C. v. Randow, 2007: Control of Dry Season Evapotranspiration over the Amazonian Forest as Inferred from Observations at a Southern Amazon Forest Site. Journal of Climate, 20, 2827-2839.
Kalnay, E., and Coauthors, 1996: The NCEP/NCAR 40-year reanalysis project. Bulletin of the American Meteorological Society, 77, 437-471.
Kousky, V. E., M. T. Kagano, and I. F. Cavalcanti, 1984: A review of the Southern Oscillation: oceanic - atmospheric circulation changes and related precipitation anomalies. Tellus A, 36, 490-504.
Larson, S., and B. Kirtman, 2013: The Pacific Meridional Mode as a trigger for ENSO in a high-resolution coupled model. Geophysical Research Letters, 40, 3189-3194.
Larson, S. M., and B. P. Kirtman, 2014: The Pacific Meridional Mode as an ENSO Precursor and Predictor in the North American Multimodel Ensemble. Journal of Climate, 27, 7018-7032.
Lee, S.-K., C. Wang, and B. E. Mapes, 2009: A simple atmospheric model of the local and teleconnection responses to tropical heating anomalies. Journal of Climate, 22, 272-284.
Lewis, S. L., P. M. Brando, O. L. Phillips, G. M. van der Heijden, and D. Nepstad, 2011: The 2010 amazon drought. Science, 331, 554-554.
Li, W., R. Fu, and R. E. Dickinson, 2006: Rainfall and its seasonality over the Amazon in the 21st century as assessed by the coupled models for the IPCC AR4. Journal of Geophysical Research: Atmospheres, 111.
Li, W., P. Zhang, J. Ye, L. Li, and P. A. Baker, 2011a: Impact of two different types of El Niño events on the Amazon climate and ecosystem productivity. Journal of Plant Ecology, 4, 91-99.
Li, C., L. Wu, and P. Chang, 2011b: A Far-Reaching Footprint of the Tropical Pacific Meridional Mode on the Summer Precipitation over the Yellow River Loop Valley. Journal of Climate, 24, 2585-2598.
Marengo, J. A., and J. C. Espinoza, 2016: Extreme seasonal droughts and floods in Amazonia: causes, trends and impacts, International Journal of Climatology, 36(3), 1033-1050,
Marengo, J. A., 1992: Interannual variability of surface climate in the Amazon basin. International Journal of Climatology, 12, 853-863.
Marengo, J. A., 2005: Characteristics and spatio-temporal variability of the Amazon River Basin Water Budget. Climate Dynamics, 24, 11-22.
Marengo, J. A., J. Tomasella, L. M. Alves, W. R. Soares, and D. A. Rodriguez, 2011: The drought of 2010 in the context of historical droughts in the Amazon region. Geophysical Research Letters, 38.
Murakami, H., and Coauthors, 2016: Dominant role of subtropical Pacific warming in extreme eastern Pacific hurricane seasons: 2015 and the future. J. Climate.
Nobre, P., and J. Shukla, 1996: Variations of sea surface temperature, wind stress, and precipitation over the tropical Atlantic and South America. Journal of Climate, 9, 2464-2479.
Poveda, G., L. Jaramillo, and L. F. Vallejo, 2014: Seasonal precipitation patterns along pathways of South American low-level jets and aerial rivers. Water Resources Research, 50, 98-118.

Rayner, N., and Coauthors, 2003: Global analyses of sea surface temperature, sea ice, and night marine air temperature since the late nineteenth century. Journal of Geophysical Research: Atmospheres (1984–2012), 108.
Richey, J. E., C. Nobre, and C. Deser, 1989: Amazon River discharge and climate variability: 1903 to 1985. Science, 246, 101-103.
Ronchail, J., G. Cochonneau, M. Molinier, J. L. Guyot, A. G. De Miranda Chaves, V. Guimarães, and E. de Oliveira, 2002: Interannual precipitation variability in the Amazon basin and sea‐surface temperatures in the equatorial Pacific and the tropical Atlantic Oceans. International Journal of Climatology, 22, 1663-1686.
Ronchail J, Bourrel L, Cochonneau G, Vauchel P, Phillips L, Castro A, Guyot JL, deOliveira E. 2005. Climate and inundations in the Mamoré basin (South-Western Amazon – Bolivia). J. Hydrol. 302: 223–238.
Rosen, R. D., D. A. Salstein, and J. Peixoto, 1979: Streamfunction analysis of interannual variability in large-scale water vapor flux. Monthly Weather Review, 107, 1682-1684.
Satyamurty P, da Costa CPW,Manzi AO, Candido LA. 2013a: A quick look at the 2012 record flood in the Amazon basin. Geophys. Res. Lett. 40: 1396–1401.
Satyamurty P, Wanzeler da Costa CP, Manzi AO. 2013b: Moisture sources for the Amazon basin: a study of contrasting years. Theor. Appl. Climatol. 111: 195–209, doi: 10.1007/ s00704-012-0637-7.
Tedeschi, R. G., I. F. A. Cavalcanti, and A. M. Grimm, 2013: Influences of two types of ENSO on South American precipitation. International Journal of Climatology, 33, 1382-1400.
Trenberth, K. E., J. T. Fasullo, and J. Mackaro, 2011: Atmospheric Moisture Transports from Ocean to Land and Global Energy Flows in Reanalyses. Journal of Climate, 24, 4907-4924.
Tedeschi, R. G., and M. Collins, 2016: The influence of ENSO on South American precipitation during austral summer and autumn in observations and models. International Journal of Climatology, 36, 618-635.
Vecchi, G. A., and Coauthors, 2014: On the Seasonal Forecasting of Regional Tropical Cyclone Activity. Journal of Climate, 27, 7994-8016.
Wang, S.-Y., R. R. Gillies, J. Jin, and L. E. Hipps, 2010: Coherence between the Great Salt Lake level and the Pacific quasi-decadal oscillation. Journal of Climate, 23, 2161-2177.
Wang, S.-Y., R. R. Gillies, L. E. Hipps, and J. Jin, 2011: A transition-phase teleconnection of the Pacific quasi-decadal oscillation. Climate dynamics, 36, 681-693.
Wang, S. Y., and A. J. Clark, 2010: Quasi‐decadal spectral peaks of tropical western Pacific SSTs as a precursor for tropical cyclone threat. Geophysical Research Letters, 37.
Werth, D., and R. Avissar, 2004: The Regional Evapotranspiration of the Amazon. Journal of Hydrometeorology, 5, 100-109.
Yoon, J.-H., and N. Zeng, 2010: An Atlantic influence on Amazon precipitation. Climate Dynamics, 34, 249-264.

Yu, J.-Y., P.-k. Kao, H. Paek, H.-H. Hsu, C.-w. Hung, M.-M. Lu, and S.-I. An, 2014: Linking Emergence of the Central Pacific El Niño to the Atlantic Multidecadal Oscillation. Journal of Climate, 28, 651-662.

Zeng, N., 1999: Seasonal cycle and interannual variability in the Amazon hydrologic cycle. Journal of Geophysical Research. D. Atmospheres, 104, 9097-9106.

Zeng, N., J.-H. Yoon, J. A. Marengo, A. Subramaniam, C. A. Nobre, A. Mariotti, and J. D. Neelin, 2008: Causes and impacts of the 2005 Amazon drought. Environmental Research Letters, 3, 014002.

Zhang, L., P. Chang, and L. Ji, 2009: Linking the Pacific Meridional Mode to ENSO: Coupled Model Analysis. Journal of Climate, 22, 3488-3505.

Zhang, W., G. A. Vecchi, H. Murakami, G. Villarini, and L. Jia, 2016: The Pacific Meridional Mode and the Occurrence of Tropical Cyclones in the Western North Pacific. Journal of Climate, 29, 381-398.

Zhang, W., G. A. Vecchi, G. Villarini, H. Murakami, R. Gudgel, and X. Yang, 2017: Statistical-Dynamical Seasonal Forecast of Western North Pacific and East Asia Landfalling Tropical Cyclones using the GFDL FLOR Coupled Climate Model. Journal of Climate, 30(6), 2209-2232.

Zou, Y., E. E. N. Macau, G. Sampaio, A. M. T. Ramos, and J. Kurths, 2016: Do the recent severe droughts in the Amazonia have the same period of length? Climate Dynamics, 46, 3279-3285.

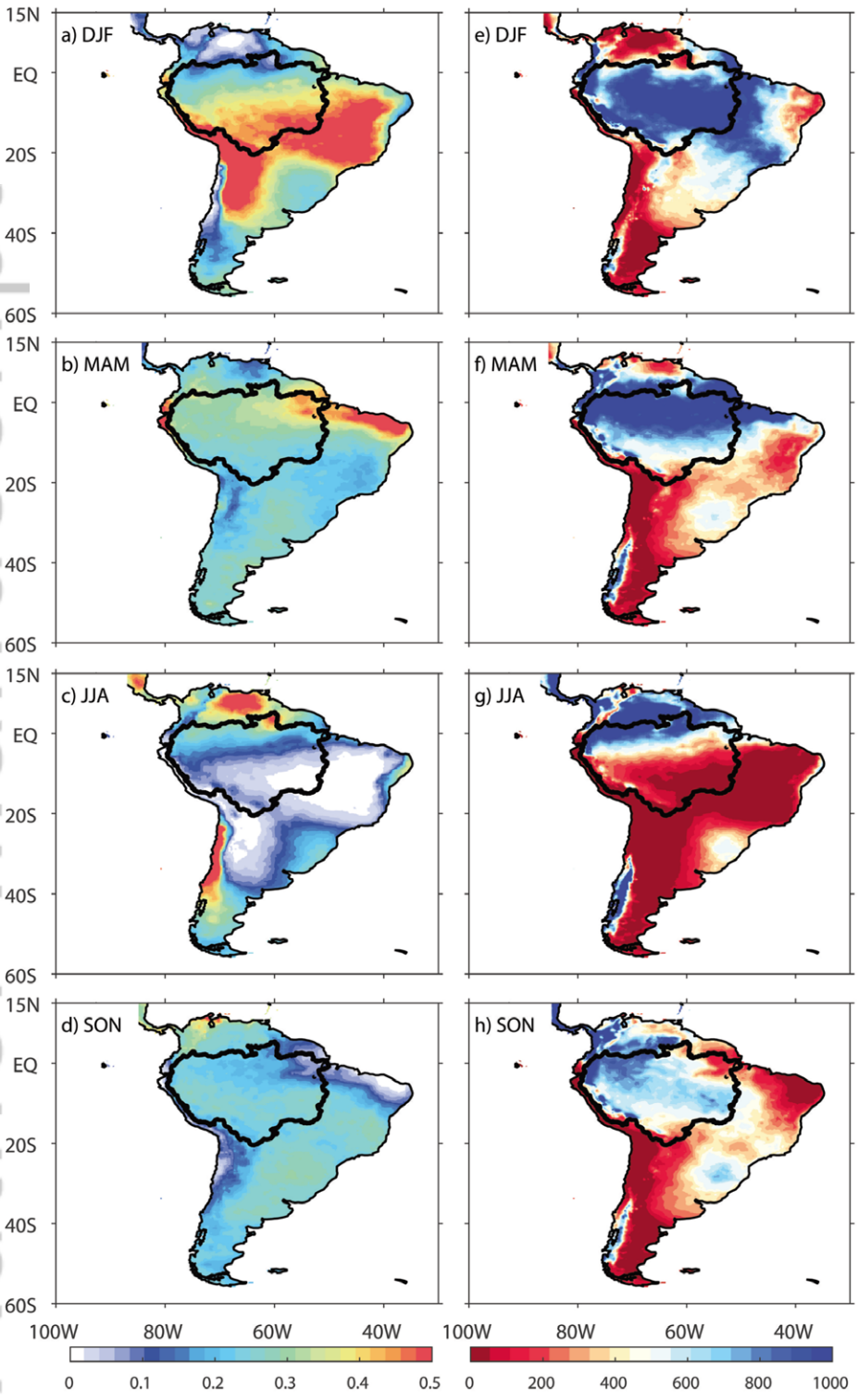

Figure 1. Proportion of the annual precipitation (left panels) and seasonal average precipitation (right panels; unit: mm) during (first row) December-February (DJF), (second row) March-May (MAM), (third row) June to August (JJA) and (fourth row) September-November (SON) "D" refers to the December of the previous year. The black boundary represents the Amazon region. Results are based on the 1979-2014 period.

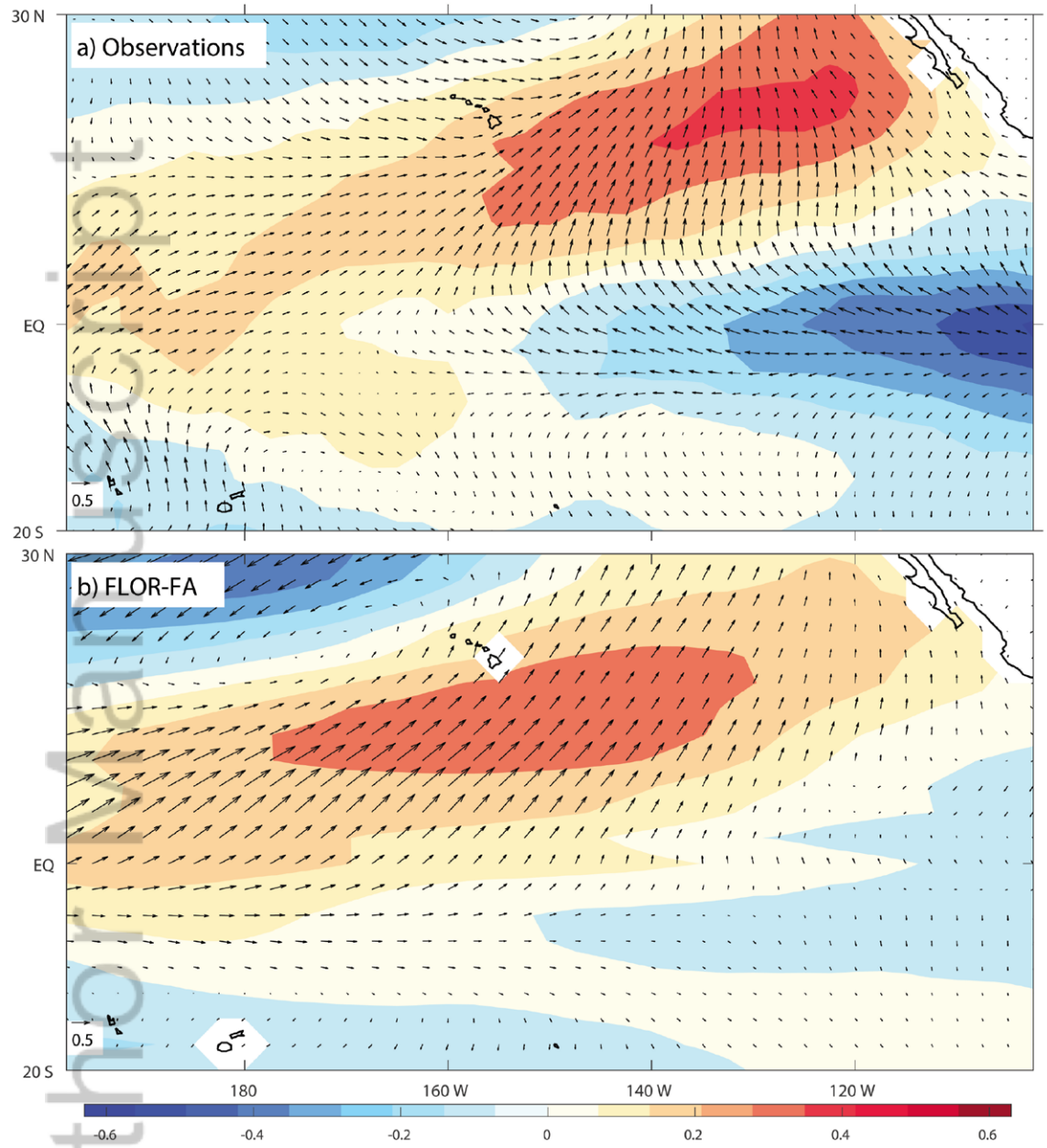

Figure 2. The Pacific Meridional Mode represented by SST (shading: unit: ºC; see color bar) and 10m surface wind fields (wind vectors, unit: ms^{-1}) in (a) observations and (b) FLOR-FA 1990 control run.

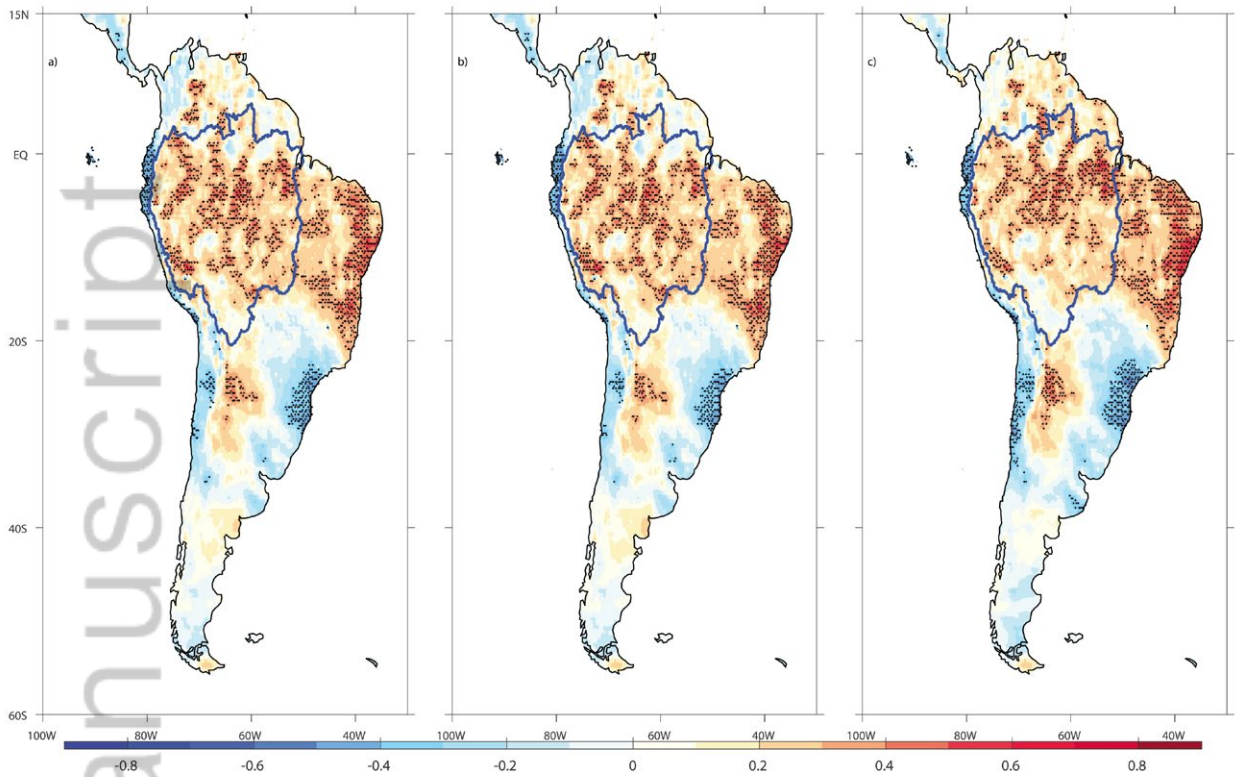

Figure 3. Maps showing: (a) the correlation coefficient (shading) between PMM and JJA precipitation; the partial correlation between PMM and precipitation by controlling for (b) Niño3.4 and (c) Niño4 in JJA. The regions with correlation coefficients that are statistically significant at 0.05 level are stippled. The blue boundary represents the Amazon region.

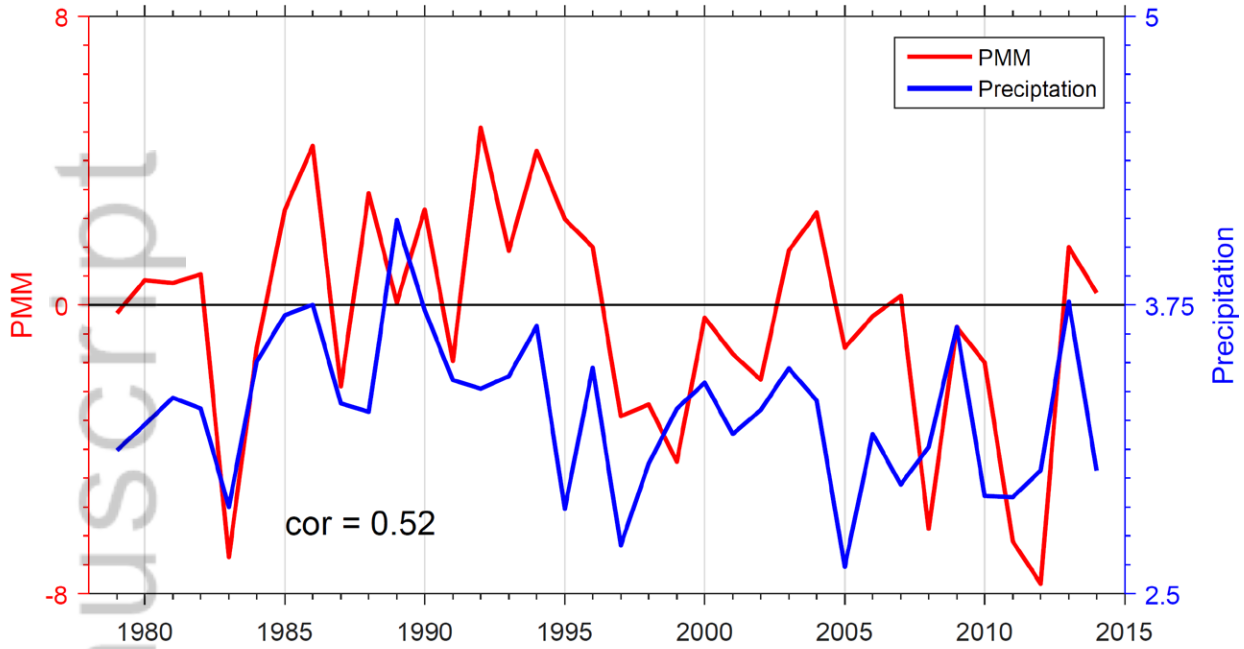

Figure 4. The time series of June-August PMM index and the precipitation (unit: mm) averaged over the Amazon basin for 1979-2014. The correlation between the two time series is 0.52 ("cor=0.52").

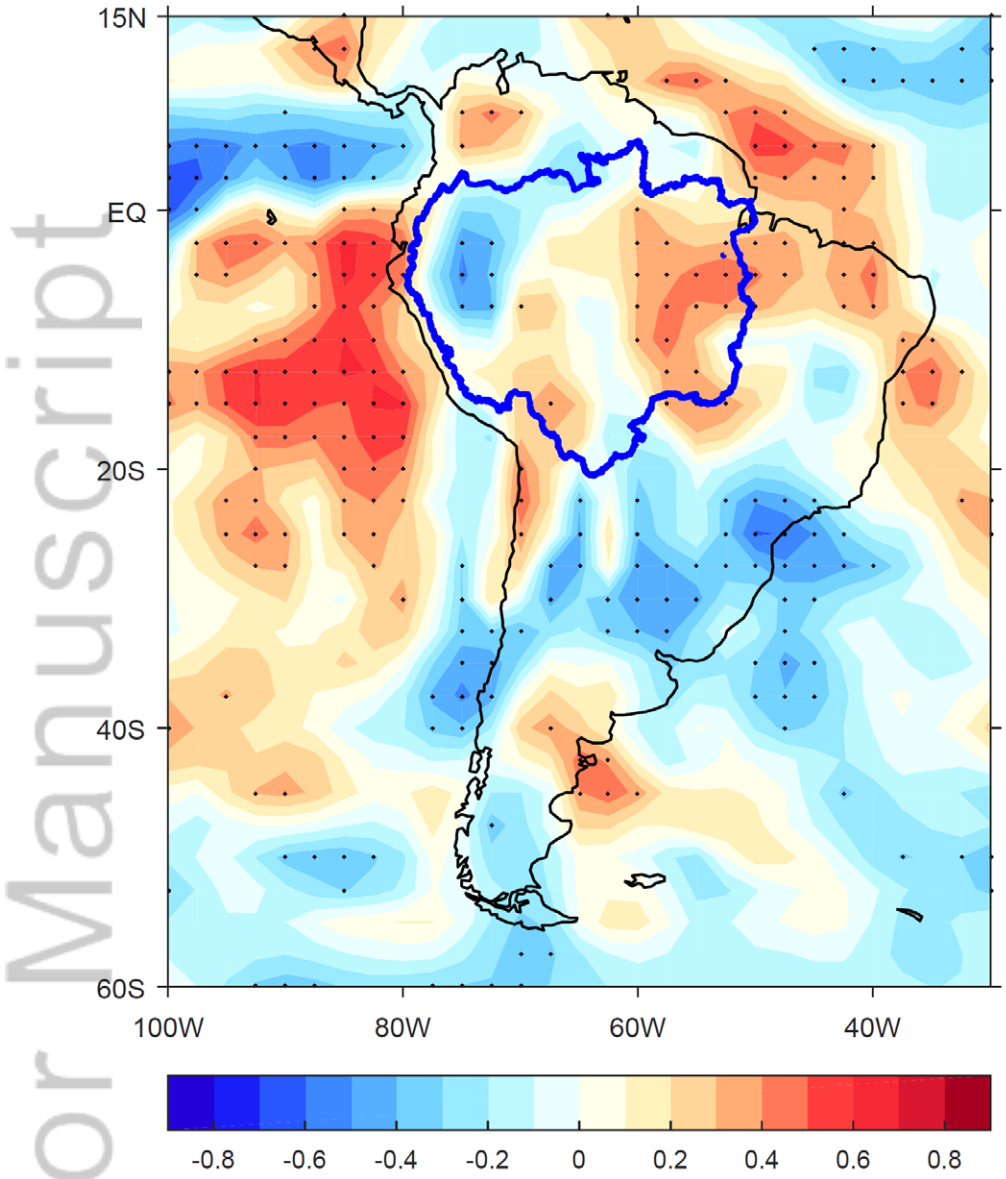

Figure 5. Correlation (shading) between the PMM index and moisture flux convergence during June-August. The regions with correlation coefficients that are statistically significant at 0.05 level are stippled. The blue boundary represents the Amazon region.

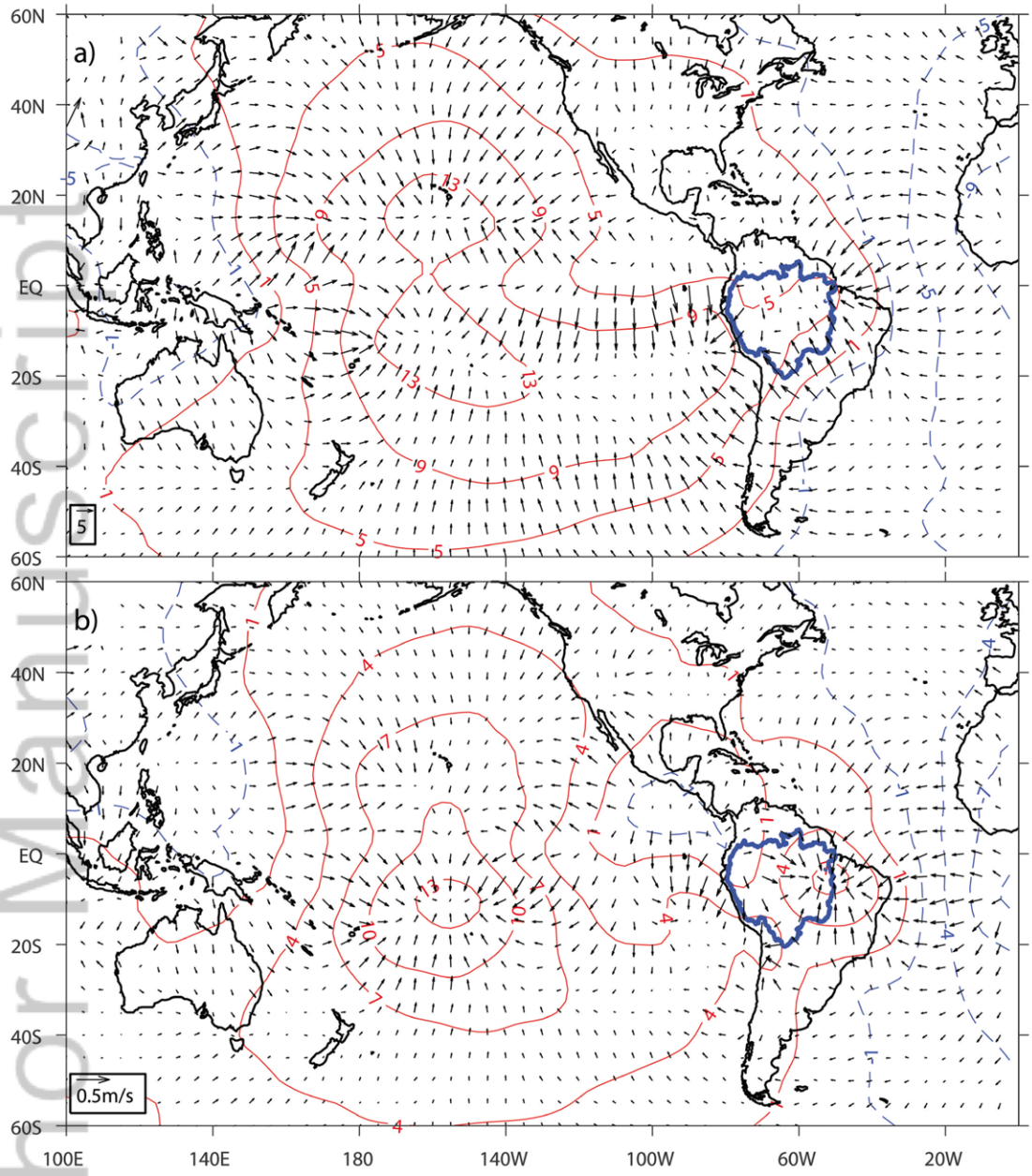

Figure 6. (a) Regression of moisture flux potential (contour, unit: $10^6 kg \cdot s^{-1}$) and divergent components (vector, unit: $kg \cdot m^{-1} s^{-1}$) onto the PMM index and (b) regression of 850-hPa velocity potential (unit: $10^5 m^2 s^{-1}$) and divergent wind (unit: ms^{-1}) onto the PMM index during JJA. The Amazon River Basin is identified with the blue contour.

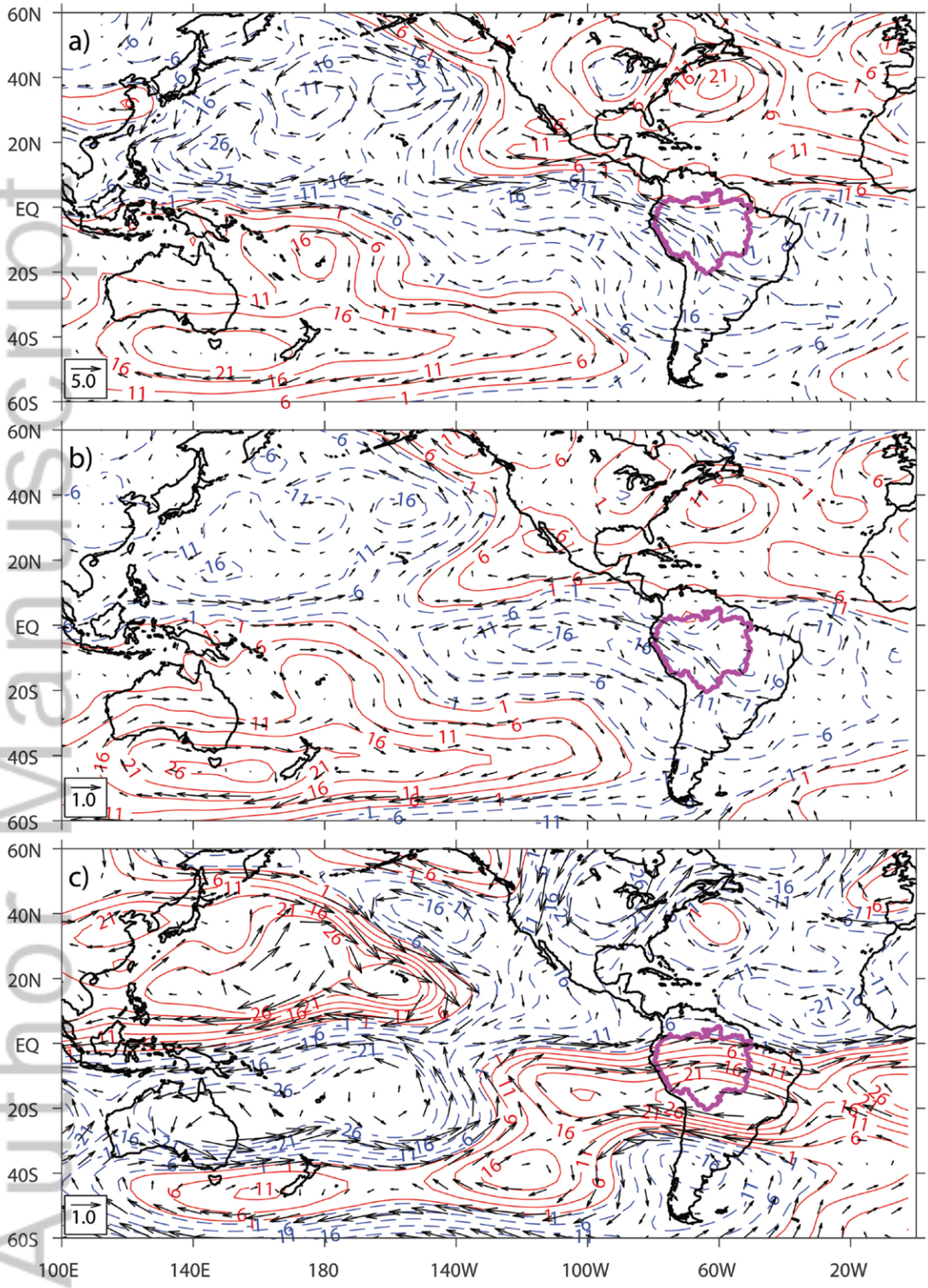

Figure 7. (a) Regression of moisture flux streamfunction (contour, unit: $10^6 kg \cdot s^{-1}$) and rotational components (vector, unit: $kg \cdot m^{-1} s^{-1}$) onto the PMM index, and (b) regression of 850-hPa and (c) 200-hPa streamfunction (unit: $10^5 m^2 s^{-1}$) and rotational wind (unit: ms^{-1}) onto the PMM index during JJA. The Amazon River Basin is identified with the purple contour.

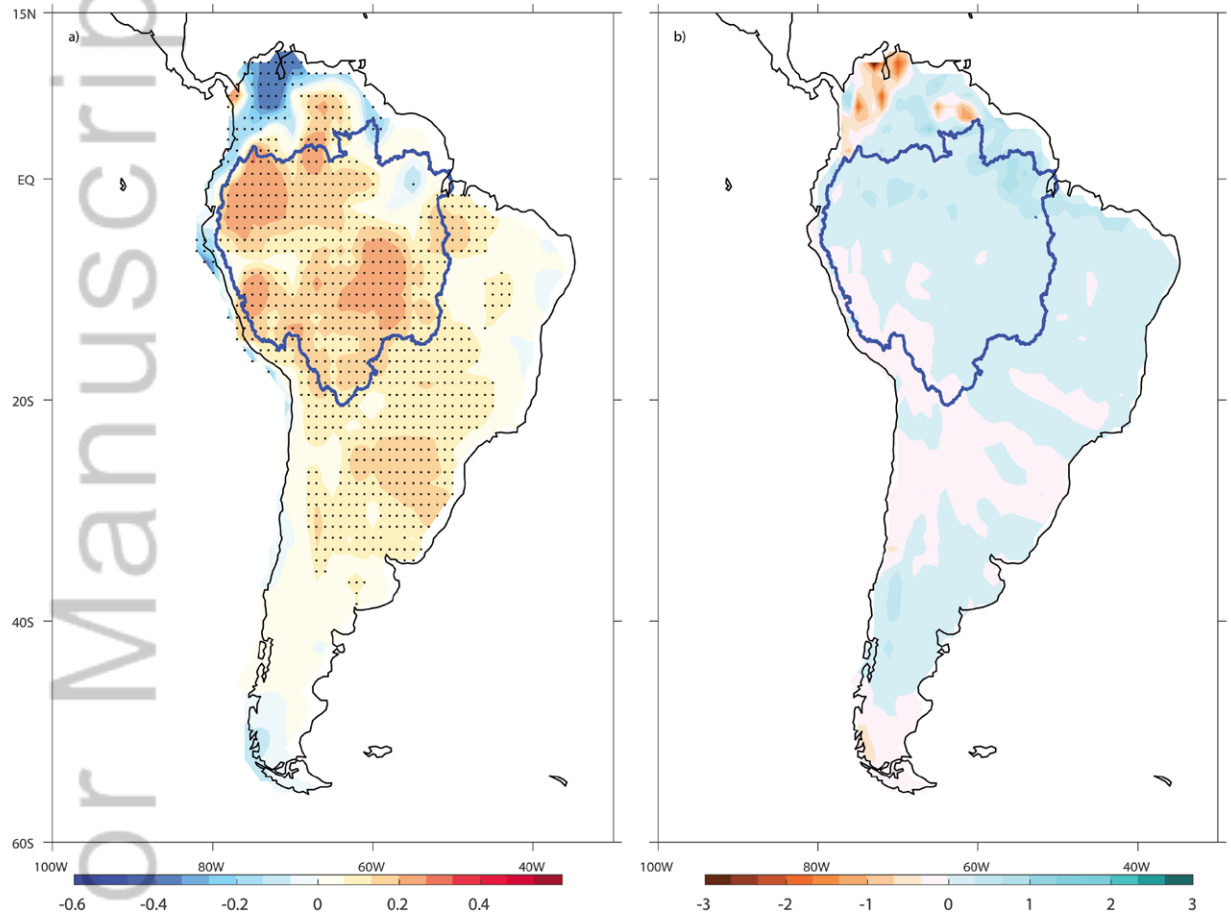

Figure 8. (a) Regression of precipitation onto PMM during JJA in the 500-year control experiment with FLOR 1990 and (b) precipitation differences (unit: mm/day) in PPMM minus CTRL experiments with FLOR. The Amazon River Basin is identified with the blue contour.

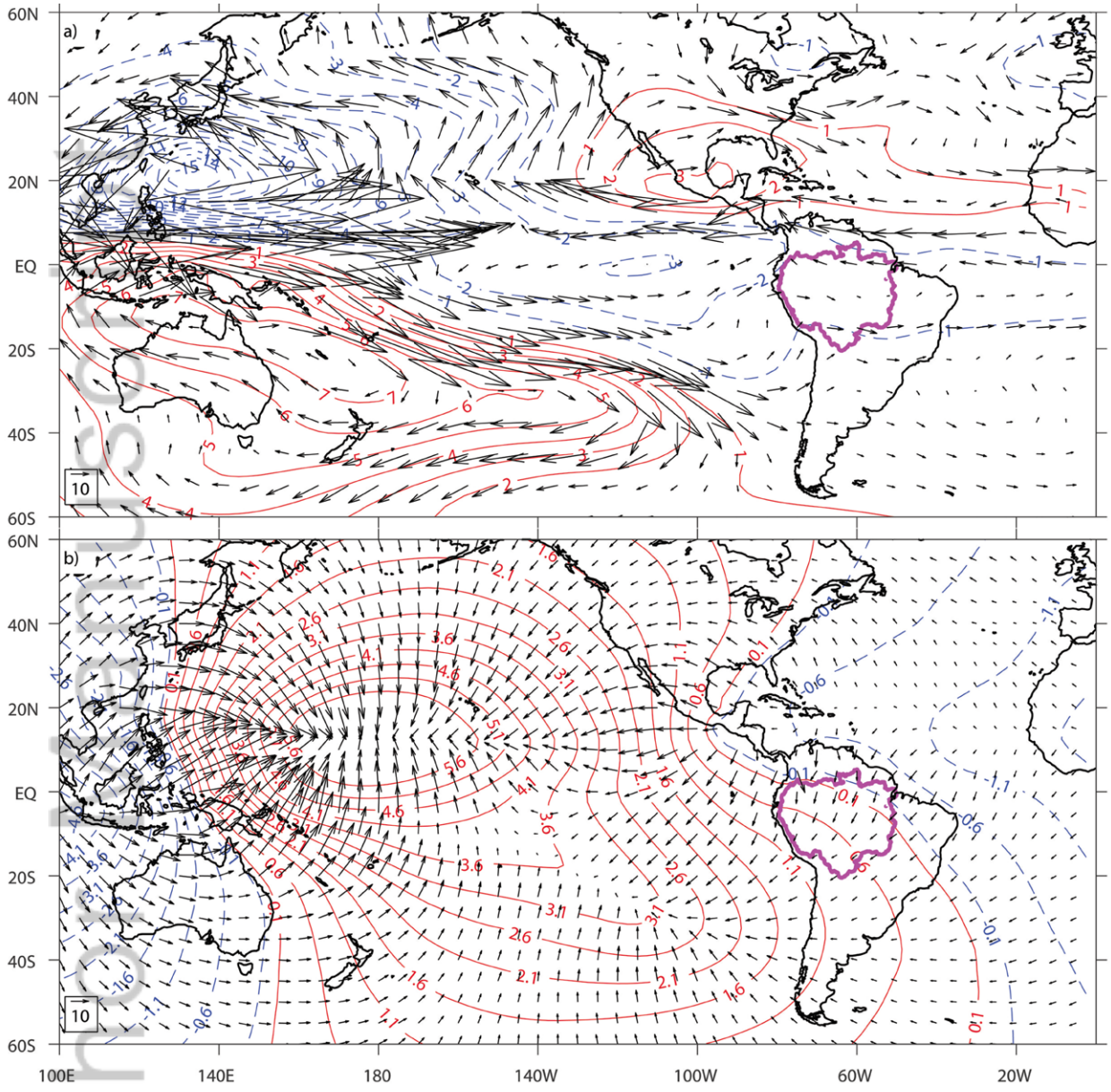

Figure 9. (a) Regression of moisture flux streamfunction (contour, unit: 10^6 kg·s^{-1}) and rotational components (vector, unit: kg·m^{-1}s^{-1}), and (b) moisture flux potential (contour, unit: 10^6 kg·s^{-1}) and divergent components (vector, unit: kg·m^{-1}s^{-1}) onto the PMM index during JJA in the FLOR-FA 1990 control experiment. The purple boundary represents the Amazon region.

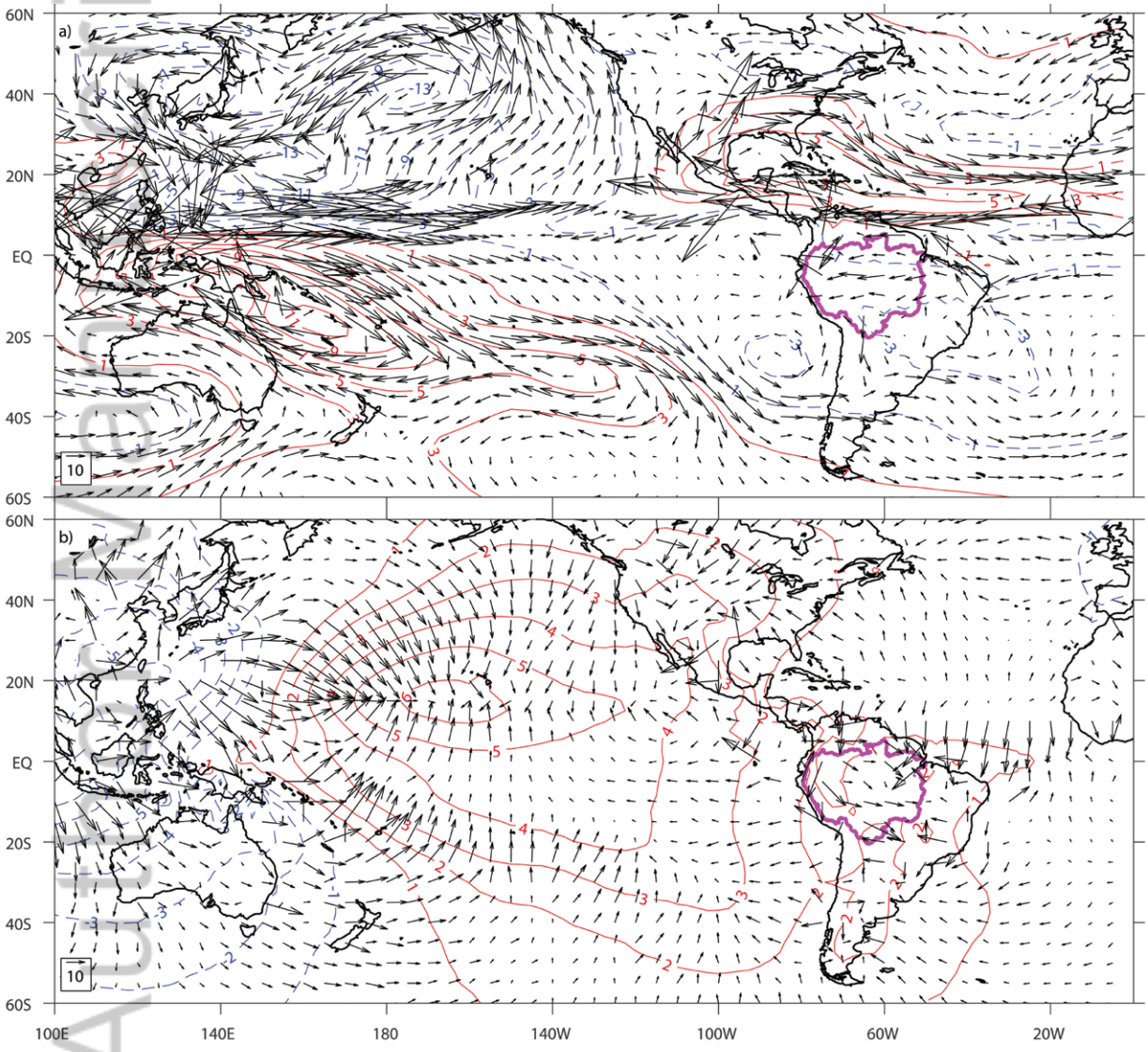

Figure 10. (a) Responses of moisture flux streamfunction (contour, unit: 10^6 kg·s^{-1}) and rotational components (vector, unit: kg·m^{-1}s^{-1}); and (b) moisture flux potential (contour, unit: 10^6 kg·s^{-1}) and divergent components (vector, unit: kg·m^{-1}s^{-1}) to PPMM (PPMM minus CTRL experiments using FLOR). The purple boundary represents the Amazon region.